SAM - a facility GLAO instrument

Andrei Tokovinin, Roberto Tighe, Patricio Schurter, Rolando Cantarutti, Nicole van der Bliek, Manuel Martinez, Eduardo Mondaca, Andres Montane

Cerro Tololo Inter-American Observatory, Casilla 603, La Serena, Chile

ABSTRACT

The SOAR Adaptive Module (SAM) will compensate ground-layer atmospheric turbulence, improving image resolution in the visible over a 3′x3′ field and increasing light concentration for spectroscopy. Ground layer compensation will be achieved by means of a UV (355nm) laser guide star (LGS), imaged at a nominal distance of 10 km from the telescope, coupled to a Shack-Hartmann wave front sensor (WFS) and a bimorph deformable mirror. Unique features of SAM are: access to a collimated space for filters and ADC, two science foci, built-in turbulence simulator, flexibility to operate at LGS distances of 7 to 14 km as well as with natural guide stars (NGS), a novel APD-based two-arm tip-tilt guider, a laser launch telescope with active control on both pointing and beam transfer. We describe the main features of the design, as well as operational aspects. The goal is to produce a simple and reliable ground layer adaptive optics system. The main AO module is now in the integration and testing stage; the real-time software, the WFS, and the tip-tilt guider prototype have been tested. SAM commissioning in NGS mode is expected in 2009; the LGS mode will be completed in 2010.

Keywords: Laser Guide Star, Adaptive Optics

1. INTRODUCTION

The 4.1-m SOAR telescope at Cerro Pachón in Chile has been conceived and built with the idea of optimizing the angular resolution. We are developing a Ground-Layer Adaptive Optics (GLAO) system to further enhance SOAR capabilities. The design of the SOAR Adaptive Module (SAM) as presented previously[1,2] has matured and is now largely implemented in the hardware, with certain sub-systems already tested. The instrument has not yet seen its first light, but it is steadily advancing towards this milestone.

The application of the SAM instrument is to increase the resolution in the visible for combating confusion in crowded fields, improving the magnitude limit, and boosting the sensitivity of integral-field spectroscopy by the increasing light concentration. It is expected to be a frequently-used "workhorse" for regular SOAR observers, so reliability and ease of operation are prime targets. An accompanying paper[3] presents the updated performance estimates* and error budget. Here we discuss new aspects of the SAM design.

2. INSTRUMENT DESIGN

2.1 SAM features

SAM will be mounted on the telescope and furnishes a turbulence-corrected beam to the science instruments, acting as an adaptor. Main features of SAM have already been described.[2] Briefly, it uses a pair of off-axis parabolic mirrors (OAPs) with $F = 810$ mm to re-image the focal plane, with image scale and exit pupil position identical to those of the bare telescope. The 60-element bimorph deformable mirror (DM) BIM-60 from CILAS reflects the collimated beam of 50-mm diameter. After the DM, the beam is split by the dichroic between the science channel (where it is refocused with OAP2) and the wavefront sensor (WFS) channel with an achromatic triplet. The WFS is of Shack-Hartmann type, with 10x10 sub-apertures and a CCD-39 detector with a SDSU controller. A frequency-tripled Nd:YAG laser ($\lambda = 355$ nm, 10W) will project a single guide star (LGS) at a low altitude, preferentially sensing low-altitude turbulence, while tip-tilt will be sensed with two natural guide stars (NGS).

E-mail: atokovinin, rtighe, pschurter, nvdbliek, mmartinez, emondaca, amontane@ctio.noao.edu

*see also http://www.ctio.noao.edu/new/Telescopes/SOAR/Instruments/SAM/ao_sam_performance.html

SAM has two focii for science instruments and, respectively, two flat fold mirrors. Switching between the focii is done by removing the first fold mounted on a translation stage. A CCD imager, SAMI, will be permanently installed at one focus, while the other focus can be used by various *visitor instruments* (VI). The atmospheric dispersion will be corrected by two Risley prisms in the collimated space after the dichroic. This space is sufficient for placing a Fabry-Perot tunable filter – a unique feature of SAM. A built-in turbulence simulator, TurSim, facilitates system check off telescope or during daytime. TurSim is capable of emulating both NGS and LGS beams.

Initially, the AO module will be commissioned with a NGS. A neutral dichroic will direct half of the light to the NGS WFS. After acquiring the experience in this mode, SAM will be re-configured for LGS operation by installing the LGS WFS (with a range-gate shutter). A UV-reflecting dichroic will direct laser photons to the WFS and isolate the science channel from the UV laser beam. Tip-tilt compensation will be provided by the SOAR tertiary mirror (up-stream of the instrument).

2.2 Interface to the telescope

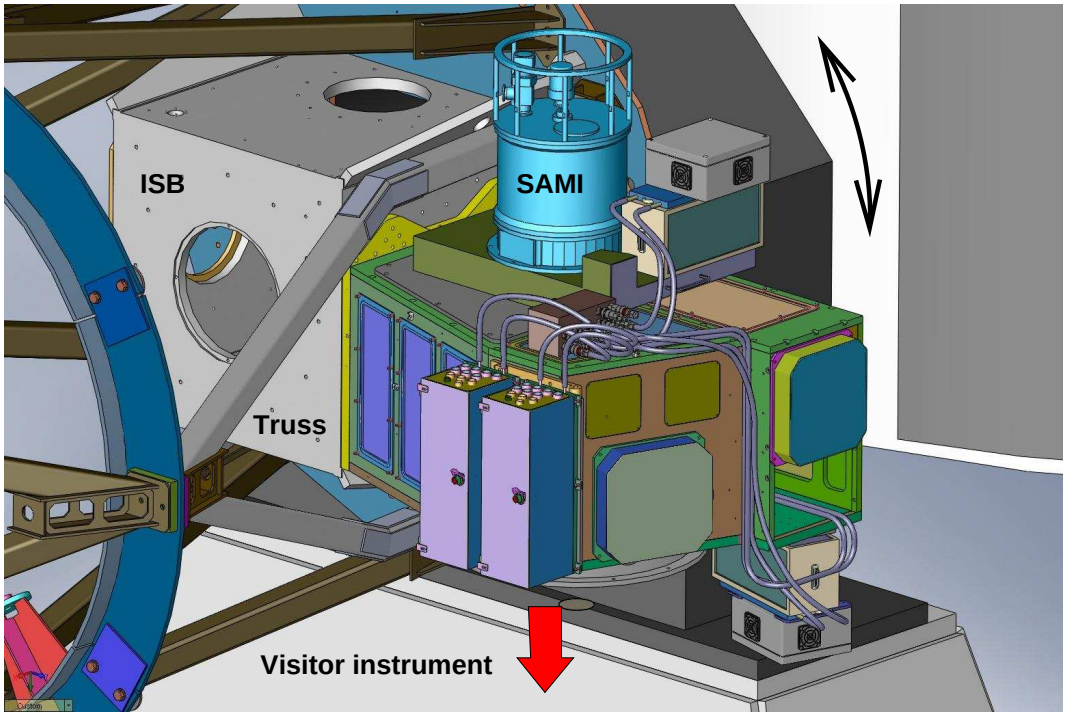

Figure 1. SAM mounted on the Instrument Selection Box of the SOAR telescope. Rotation of the ISB is shown by the arrows.

The SAM is mounted at the Nasmyth focus of the SOAR on a cubic steel structure called Instrument Selection Box (ISB), see Fig. 1. SAM receives the light after 3 reflections in the telescope and one reflection inside the ISB. As the ISB rotates to compensate for field rotation, SAM also rotates with respect to the gravity. The space available for SAM and its science instruments is restricted by this rotation, by the Nasmyth bearing on one side and by the axial instrument (Goodman spectrograph) on the other. As if this were not enough, the ISB is surrounded by a truss structure. One truss member will be modified or removed to enable SAM installation. Tight space restrictions complicated the mechanical and optical designs of SAM, which had to be optimized for packaging (see below).

The initial allocation of 340 kg for the mass of SAM (including a 55-kg VI) was motivated by the total ISB load limit of 3000 kg. SAM meets this budget, but can hold a heavier VI if allowed by SOAR.

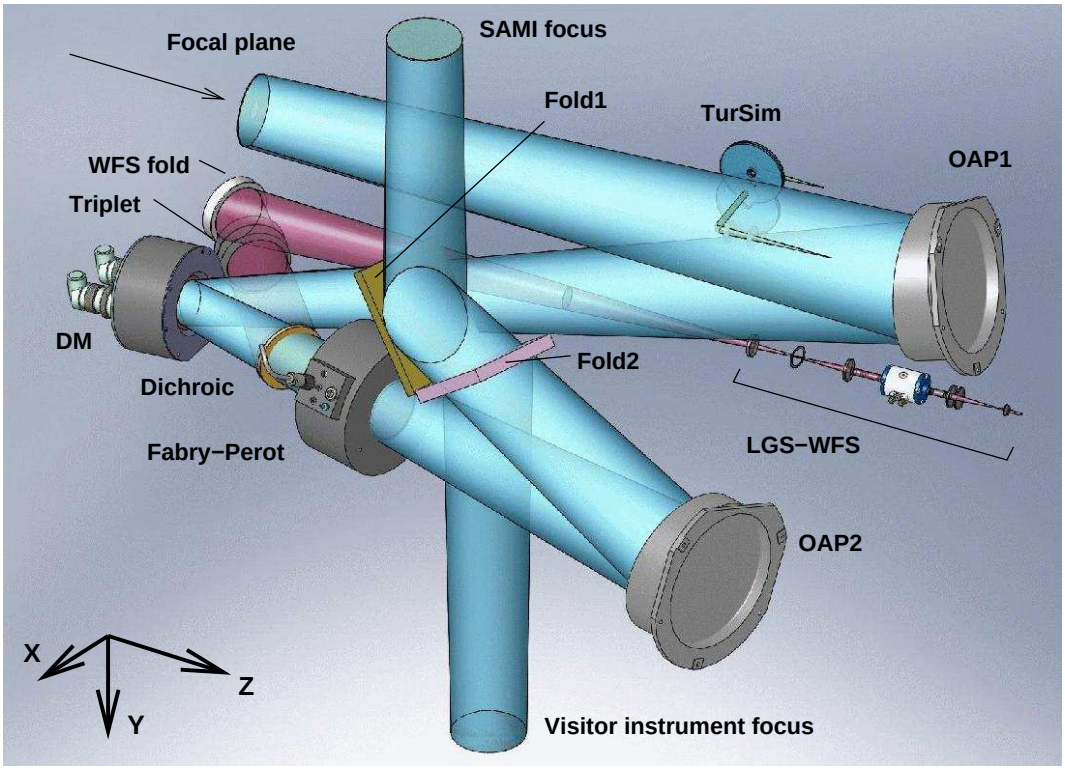

Figure 2. Optical layout of SAM. Two guide probes in the focal plane are not shown.

2.3 Optical design and packaging

Figure 2 shows the optical design of SAM. The nominal distance of the telescope focal plane from the ISB mounting surface is 150 mm, so the DM would collide with this surface. To move the focal plane away without refocusing SOAR, we displaced the incoming beam by 67.5 mm with respect to the ISB center. This was possible because the folding mirror inside the ISB (M4) has not yet been designed, so we moved it by 67.5 mm towards the telescope. The displacement of the whole SAM reduces the bending moment exerted on the ISB. The center of mass is placed as close to the flange as possible to reduce the torque.

The optical design has two free parameters – the clocking angle of the beam deflection by OAP1 θ_{AZ} around the axis of the incoming beam, Z, and the incidence angle on the DM θ_{DM}. We used this freedom to optimize the location of the elements. To simplify the mechanical design, we placed all elements except OAP1 and the science fold mirrors in one plane parallel to XZ, as though they were on an optical table. The location of the science fold mirror at the expected mass center of SAM was set as a target and the two angles were optimized with Zemax to minimize the distance from the target. We tweaked a little the resulting angles, selecting finally $\theta_{AZ} = 65°$ and $\theta_{DM} = 14°$.

Both optical (Zemax) and mechanical (Solid Works) design tools use the same global coordinate system with the origin at the center of the SOAR focal plane. The optimized optical layout naturally leads to a "two-storey" housing design. The upper floor contains the SOAR focal plane, two tip-tilt guiders, OAP1 and the TurSim. The lower floor holds all other elements. The science fold mirrors are located between the floors, near the center of the SAM structure.

The dichroic will reflect the UV light (in the case of LGS) or 50% of all light (in the case of NGS) to the WFS path. The dichroic mount provides for an easy exchange of those dichroics without disturbing their alignment. The WFS beam is focused by a cemented apochromatic UV triplet of 80 mm diameter and $F = 500$ mm and folded by a flat mirror on a path parallel to the incoming beam. The triplet was optimized for LGS altitudes from 7 km to 14 km, while giving diffraction-limited images of NGS at infinity as well. The NGS WFS module

consists of a reflecting aperture plate with a rectangular opening (to permit acquisition by observing the reflected star), a simple 2-element collimator, and a lenslet array (LLA) mounted in front of the CCD.

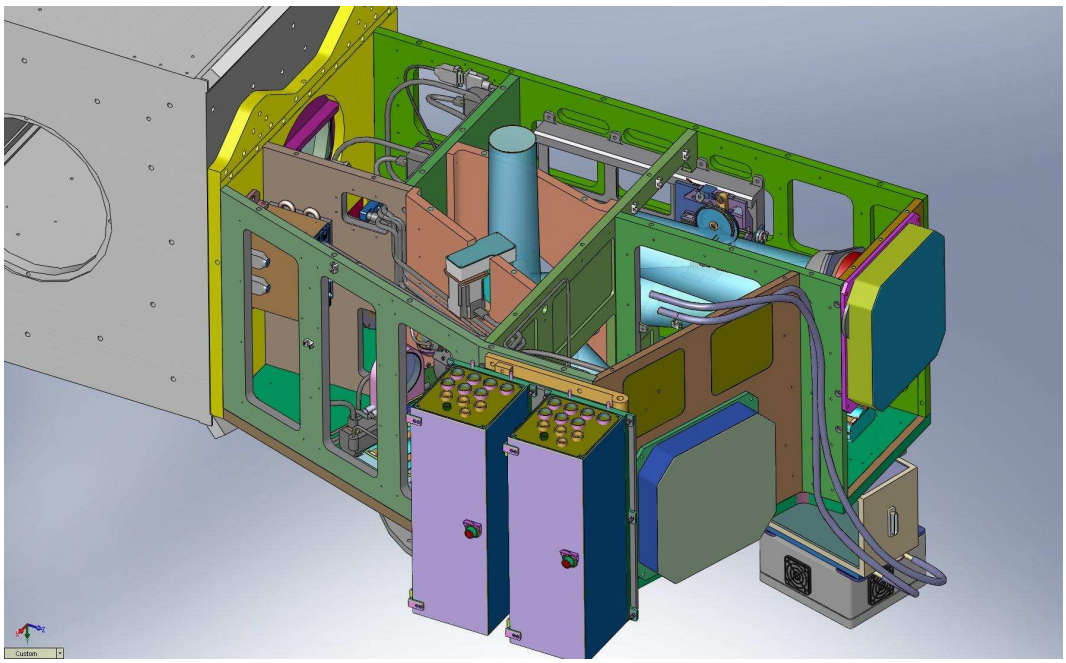

Figure 3. SAM mechanical structure ("bench") mounted on the ISB.

In the LGS WFS, the first element (a singlet) will be located in front of the aperture, followed by the collimator, Pockels cell between crossed polarizers, and another two lenses. The beam diameter at the Pockels cell is 6.49 mm. Despite a large difference in the ray path between two extreme LGS altitudes, 7 km and 14 km, the diameter of this collimated beam and the size of the pupil on the LLA are kept constant by adjusting the distance between the first lens and the focal aperture plate. The whole WFS is mounted on a translation stage for focusing. By fine adjustments of the WFS focus in closed loop, we can fine-tune the focus of the science beam.

2.4 Mechanical design

The SAM housing is a rigidized aluminum frame. It is densely populated by optical components in their cells, mechanisms, motors, and cables as shown in Fig. 3. Special attention was given to providing access to all elements through rectangular holes in the walls of the housing, covered by light-weight panels.

The flexure of the housing loaded with SAMI and a 55-kg VI was evaluated at each 10° of the ISB rotation (Fig. 4). It is not trivial to deduce the image displacement in the science focus caused by flexure because, apart from the housing deformation, it depends on the reflections inside SAM, and even a small change of the angle of OAP1 or DM can cause substantial shifts. We estimated the effect of internal reflections by taking suitable nodes of the finite-elements model as representative of the mirror angles and calculating beam displacements caused by these angles. The requirement of image displacement of less than 24 μm for each 10° of ISB rotation is met, the actual displacements do not exceed 13 μm.

The thermal expansion of the aluminum housing matches the temperature variations of the OAPs focal length because they are made of the same material. The rigid coupling between aluminum housing and steel ISB does produce thermal stress, which is however acceptably small and does not affect the optics because it is located far from the mounting plate.

Electronic components such as motor controllers are located in two boxes attached to the outside of the housing. The heat generated by this electronics, the WFS CCD, two CCD controllers, and the tip-tilt light detectors, will be removed by the glycol line.

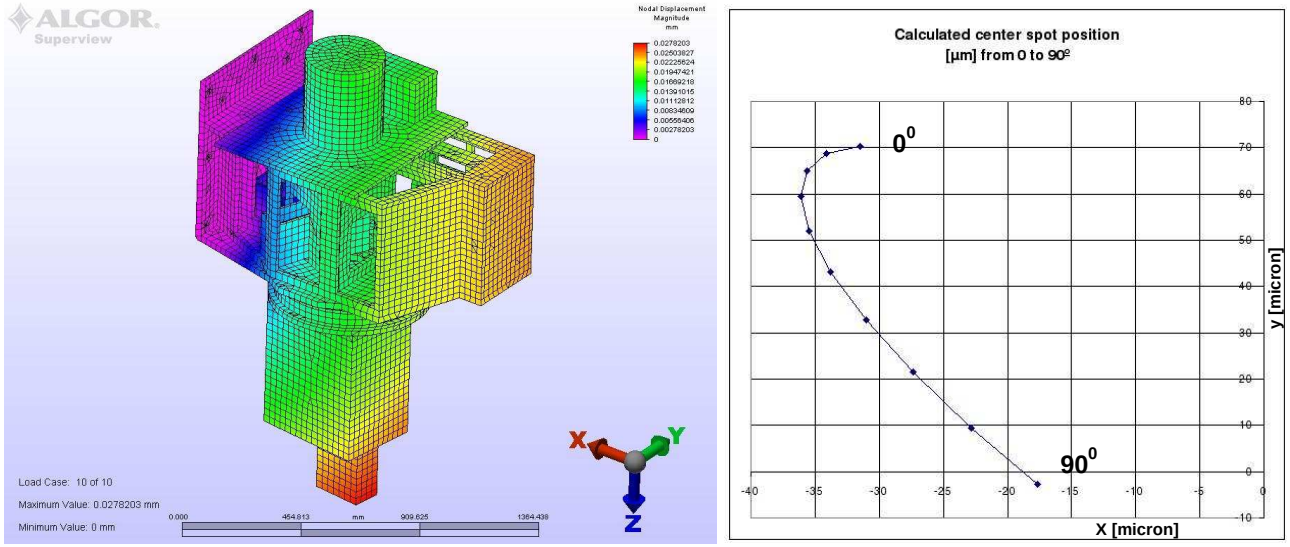

Figure 4. Flexure analysis of the SAM housing with the imager and visitor instruments attached. Left: SAM structure deformations with colors corresponding to the displacements from 0 (violet) to 28 μm (red); note that the coordinate system is different from Fig. 2. Right: calculated image displacement in the SAM focal plane for ISB rotation from 0° to 90°.

2.5 Tip-tilt guiders

In the LGS mode, SAM will use two natural guide stars for tip-tilt compensation. The stars will be selected outside the science field, ideally straddling it. Two tip-tilt stars produce a more uniform PSF over the field, compared to just one star.

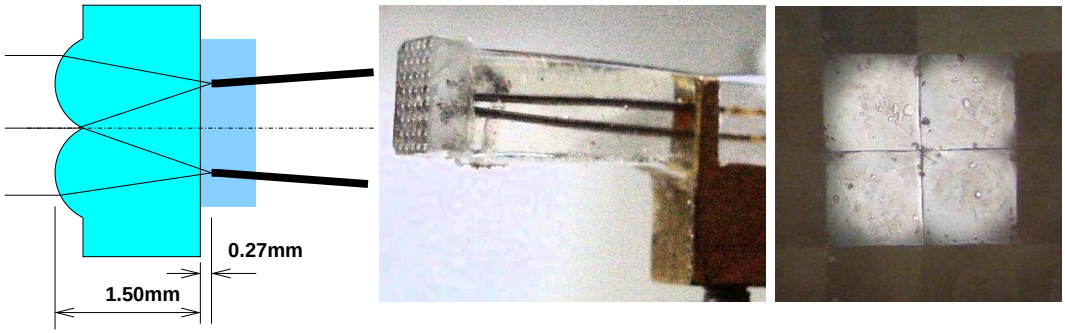

Figure 5. Splitting the stellar image into 4 quadrants with micro-lenses and fiber optics. Left: optical principle, center: prototype splitter, right: quadrants back-illuminated through the fibers.

As in many AO systems, the tilt is sensed by splitting the stellar image into 4 quadrants and detecting the photons with avalanche photo-diodes (APDs). We use 4-APD modules SPCM-AQ4C from Perkin Elmer. These devices are not protected against over-light conditions which can happen despite all precautions. We made a custom protection circuit that shuts down the 30 V power source when the avalanche current exceeds a certain threshold. This device has already saved our APDs during tests at the telescope.

The stellar image falls onto a 2x2 micro-lens array, with fiber inputs located at the lens focii (Fig. 5). The light is brought to the APDs through 1-m optical fibers with a core diameter 100 μm and standard FC connectors. We use acrylic micro-lenses with a focal length of 1.2 mm, so the 100 μm fiber core can accept an $F/12$ or slower beam. The 0.5 mm square micro-lens corresponds to 1.5″ on the sky when placed at the $F/16.6$ SOAR focus, so the 2x2 fiber splitter has a 3″ field-of-view. The fibers are slightly inclined to collect more light from the center of the field, where the star will normally be kept. All 4 fibers are glued into steel ferrules and polished. They are

co-aligned with the lenses during assembly, then potted with transparent epoxy to form a single solid module. The opposite ends of the fibers are fitted with FC connectors. The transmission of such custom-made splitter is about 70% as measured in the laboratory. It could be better if micro-lenses with a better surface quality were used. The local surface defects of the lenses are seen in Fig. 5 (right) as dark spots. The dead zone between the lenses is $<50\,\mu$m, negligible compared to the size of the stellar image. Acrylic micro-lenses do not transmit the UV light from the LGS, thus protecting the APDs.

The prototype guider was tested at SOAR. A star of magnitude R gives the counting rate $F = 10^{10.76-0.4R}$ photons/s from all 4 channels together. The dark count at room temperature is from 100 to 200 Hz per APD, comparable to the dark-sky flux. The rms error of the tilt measurements can be estimated as $\sigma = 0.533\varepsilon(N + B)^{0.5}/N$, where ε is the FWHM of the Gaussian stellar image (seeing), N and B are the total numbers of photons from the star and the background, respectively, for one correction cycle. For example, $\sigma = 28$ mas is reached for an $R = 18$ star under $0.8''$ seeing with 10 Hz closed-loop bandwidth. This performance is acceptable for SAM and ensures a nearly complete sky coverage.

Each of the two fiber splitters is mounted inside a small guide probe, with a 3-mm right-angle prism in front of it. Behind this assembly, there is another prism and a single-mode fiber which can project light inside the instrument, thus creating an artificial point-source image coincident with the center of the micro-lenses. This fiducial source will be used to reference the probe location and focus, but also for alignment and optics control, taking advantage of the remotely controlled motions of the probes in X,Y,Z. Each probe can reach the center of the field. The collision between the probes will be prevented by the software, but we have also developed a hardware anti-collision protection (a permanent magnet in one probe and a Hall sensor in another).

2.6 Software

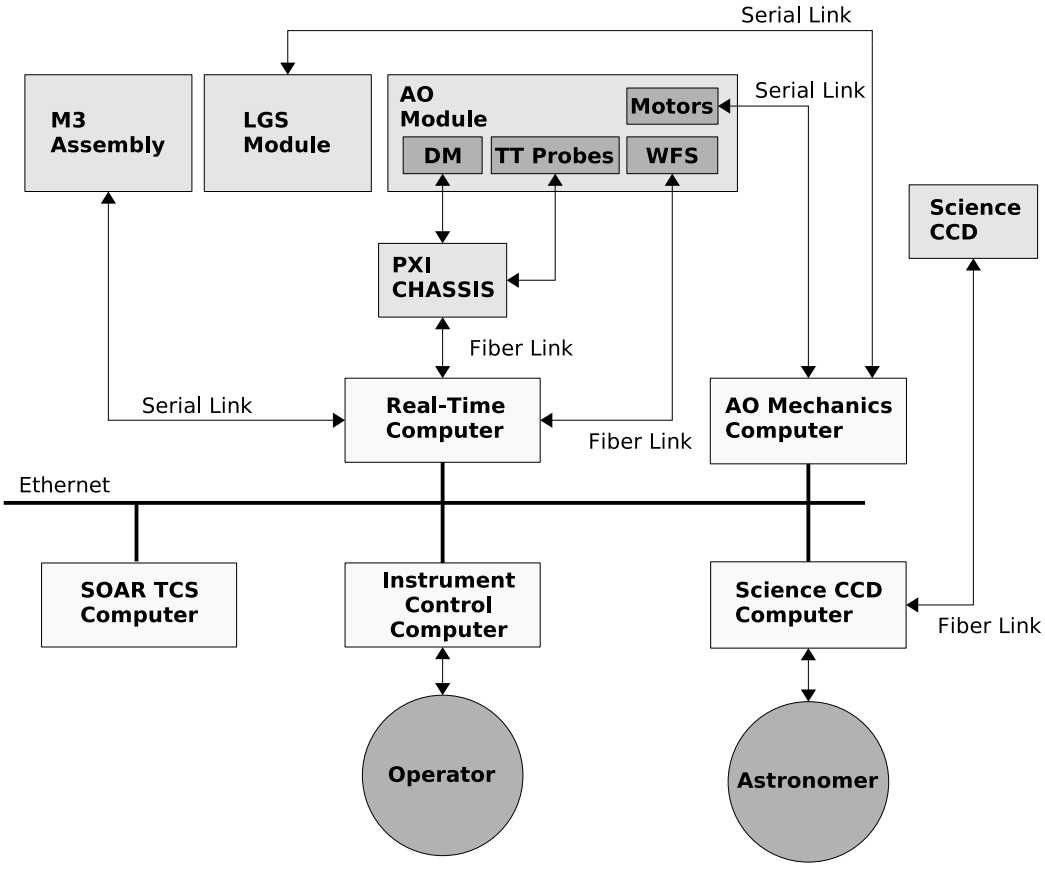

Figure 6. SAM computing system.

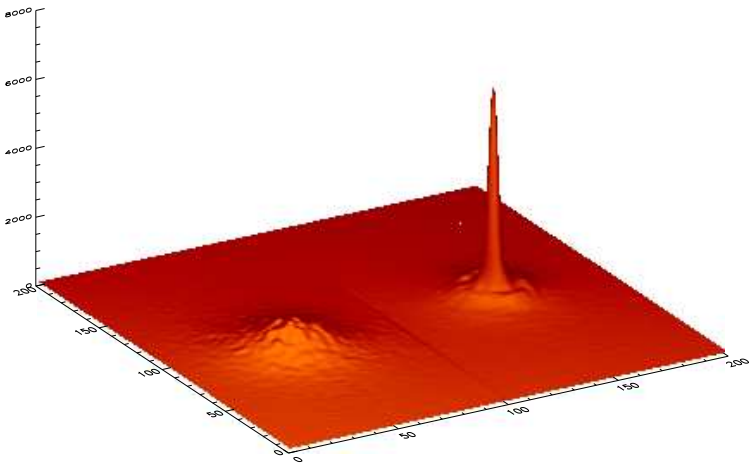

Figure 7. Long-exposure PSFs recorded with TurSim, NGS WFS, and SAM software in the laboratory prototype. Left: open loop, FWHM 0.40″. Right: closed loop, FWHM 0.06″. The simulated seeing was 1″, but the open-loop PSF is narrower because the phase screens have less power in the low-order modes compared to atmospheric turbulence.

The SAM computing environment is distributed in 4 different processors, each one running a specific software module: the Real Time Computer (RTC), the AO Mechanics Computer (AOMC), the Instrument Control Computer (ICC), and the SAM Imager Computer (Fig. 6). All computers are standard desktop PCs running Linux. The RTC is a special case, it runs a patched version of the Linux kernel to support RTAI real-time extensions in order to meet the requirements of low latency and jitter.

The RTC runs the real-time software that actually closes the loop over the WFS, DM mirror, SOAR M3 mirror (tip-tilt correction), SOAR mount, and the laser launch telescope (LLT). The AOMC controls and monitors all mechanisms, calibration light sources, and instrument parameters such as power supply voltages and temperature.

The ICC provides supervisory control over the RTC and AOMC. The operator interacts mostly with this computer while doing observations. The SAMI computer controls the dedicated imager, to be replaced by the visitor-instrument control computer when needed.

The **real-time software** continuously measures atmospheric distortions and compensates them. At the core of this software module is a real-time kernel module that processes the Shack-Hartmann images acquired by the WFS CCD to measure slopes and derive control signals for the DM, M3, LLT and mount. A high-level program written in Labview provides the interfaces for monitoring, calibration, and external commands.

The real-time core is driven by the interrupt handler of the WFS CCD controller. Each controller interrupt triggers the control algorithm. When the control loop is open, only the slopes are measured; when it is closed, the slopes are multiplied by the reconstructor matrix, and the result is filtered by the temporal controller before being sent to the DM. The algorithm supports two temporal controllers: a simple integrator and the Smith predictor (SP). The SP out-performs the integrator under high-flux conditions.

The real-time core also computes the commands to SOAR M3 for tip-tilt compensation. Depending on the operation mode (NGS or LGS), the core obtains the tip-tilt error signals from the WFS or from the tip-tilt probes, respectively.

The real-time software has been tested with TurSim emulating the NGS mode in the laboratory prototype, with the real CCD and DM (Fig. 7). In a 3.2 GHz P-IV class computer, the DM control signals can be computed and generated in less than 0.5 ms. The algorithm supports two centroiding methods to measure the slopes: correlation and weighted center of gravity.[4] Under laboratory conditions, the minimal acceptable flux was found to be around 100 photons per loop cycle, with the readout noise of 9.85 electrons. In terms of the RMS centroid error, the weighted center of gravity showed better performance in the low-flux regime, while the correlation showed better performance in the high-flux regime.

The loop data (WFS slopes and DM commands) can be saved for further off-line analysis. They are also processed in real time to estimate the seeing and the atmospheric time constant. The software offers a rich set of diagnostic tools for monitoring spot parameters, DM commands, Zernike modal coefficients and their statistics, etc.

3. LGS SYSTEM

3.1 Laser and return flux

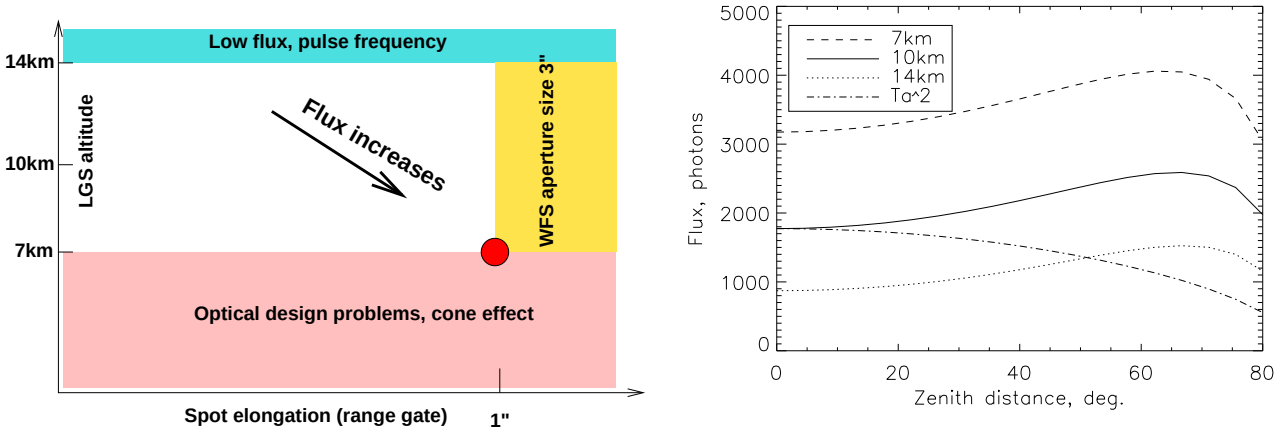

Figure 8. Left: the trade space of the LGS parameters, range and spot elongation. Right: return flux calculation (the dash-dotted line shows the atmospheric absorption relative to zenith)

SAM will use a commercial pulsed UV laser Q301-HD from JDSU, of the type employed in material processing. UV radiation is well scattered by the air and is easy to separate from the science wavelengths. The safety thresholds for the UV are much higher than for the visible. As a result, the SAM beam does not pose any threat to airplanes passing through it. As a down-side, the overall optical transmission is lower in the UV than in the visible.

The 10 W laser power is selected after several trade studies to balance conflicting requirements and to leave some margin. The return flux increases when the LGS is focused at a lower range H and when the range-gate pulses are longer (Fig. 8, left), but there are restrictions imposed by the optics (it is difficult to re-image the spot closer than at 7 km) and by the WFS field (3″x3″). The laser pulse repetition frequency 10 kHz corresponds to the round-trip time to 15 km altitude, so the LGS must be lower to avoid pulse overlap. We will select initially the 1″ elongation at the outermost apertures and $H = 7$ km (range-gate pulse of 0.79 μs duration), but will keep the possibility of changing these parameters later. The return flux per sub-aperture and per 4.2 ms loop cycle is calculated in Fig. 8 (right) as a function of the zenith angle z for three values of H. A total transmission of 0.1 is assumed, accounting for the light losses in the emission and reception. The atmospheric absorption in the UV is non-negligible and increases with z (dash-dotted line in Fig. 8, right) but, despite this, the return flux actually increases with z because higher air density more than compensates for the absorption.

3.2 Pockels cell shutter

In the LGS mode, the return light will be gated in the WFS with a Pockels cell shutter. We use an off-the-shelf KD*P cell QX1020 from Cleveland Crystals because of its low "ringing". This phenomenon is caused by mechanical oscillations excited in the crystal by the driving pulse and can be modeled as a resonator response. It turns out that the ringing caused by the main resonance of this cell at 95 kHz is not troublesome for short ($< 1\,\mu$s) pulses, but a small after-pulse caused by higher-order resonances is always present. It is delayed by 3.5 μs from the driving pulse and contains 20% of the light transmitted in the main pulse (Fig. 9). This after-pulse influences mostly the shape of the laser spots in the inner sub-apertures and produces a small seeing-dependent bias in the inner-spot centroids, ranging from 9 mas to 30 mas for the seeing from 0.8″ to 1.2″.

The Pockels cell shutter works with linearly-polarized light. The polarization is preserved by the Rayleigh scattering, but the laser projector and SAM rotate relative to each other because SAM is mounted on the rotating ISB. We will convert the laser beam to circular polarization before the launch telescope. The incoming

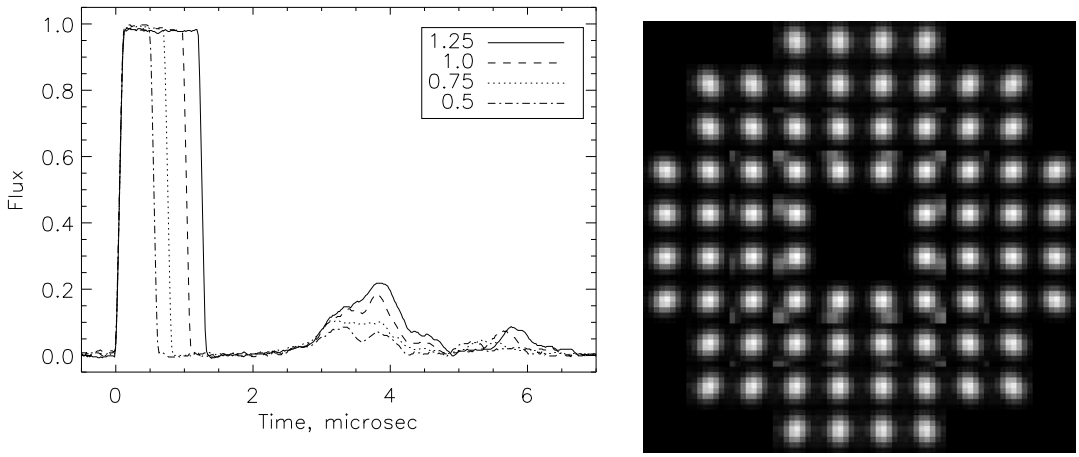

Figure 9. Transmission of the Pockels-cell shutter vs. time for pulses of different length (in μs, see legend) and simulated spots in the S-H WFS including the effects of diffraction, seeing, 1″ spot elongation, and ringing (right).

circularly-polarized beam will be transformed again in the LGS WFS into linear polarization by a $\lambda/4$ phase plate placed in the collimated beam before the first polarizer.

3.3 Beam transfer and laser launch telescope

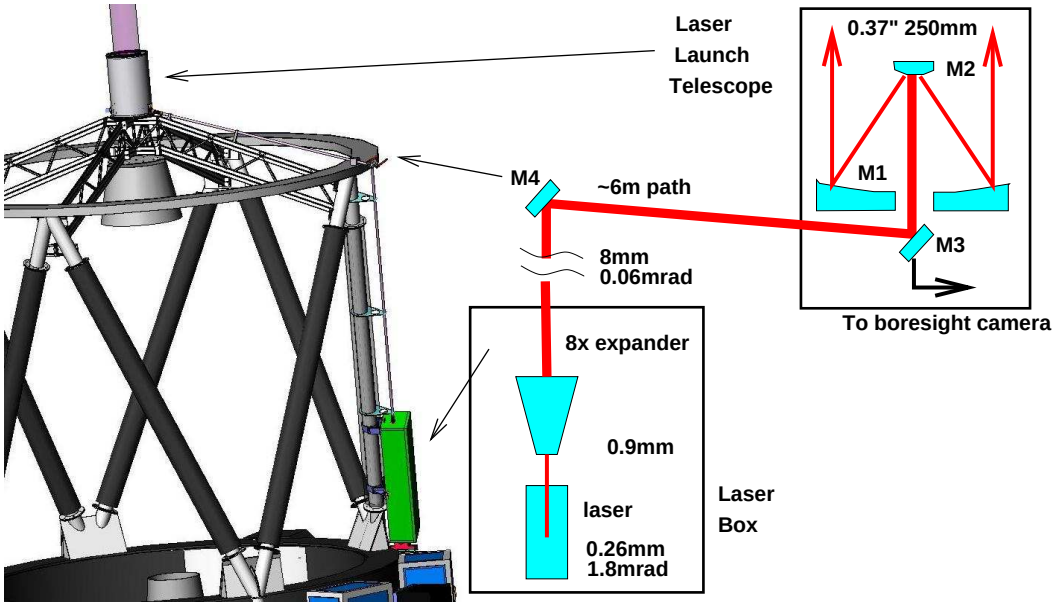

Figure 10. Scheme of the laser beam transformations (not to scale). The beam parameters (diameter 2ω and full divergence 2θ at $1/e^2$ level) are indicated. The picture on the left shows location of the LGS elements on SOAR.

The laser is small (mass 14.5 kg), and can work in any orientation with respect to the gravity, but needs temperatures above 15°. The laser will be placed in a closed and thermally-stabilized box mounted on the telescope truss. The beam will be expanded 8 times to match it flexibly with the LLT optics, and transmitted over a distance of ∼6 m to the top of the telescope with just one reflection from the mirror M4 at the SOAR top

ring. The beam path will be enclosed in tubes. Figure 10 shows schematically the main elements of the beam transport system. The tilt of M4 will be remotely controlled to compensate for flexure, if necessary.

The LLT optics consists of a 15-mm spherical secondary mirror M2 and a 300-mm elliptical primary M1. The LLT magnifies the beam size by 33 times and reduces its tilts by the same amount. Diffraction-limited image quality (Strehl ratio > 0.8 at 355 nm) is maintained only in a small field of $\sim 30''$ radius. Although the flexure of the SOAR telescope, as measured, is much less than that, we will provide LLT pointing over a range of several arc-minutes by tilting the primary mirror around its focus, so that the image quality is preserved. Fast tracking of the LGS spot will be achieved by mounting the flat diagonal mirror M3 on piezo-actuators. Such tracking is needed to compensate for the tilts of the return beam introduced by the SOAR tip-tilt mirror and, eventually, potential vibrations of the LLT. However, the estimates derived from the SOAR guider indicate that vibrations are not likely to present any problems. In this respect, it is essential that the beam entering the LLT be collimated, so that the displacement of the LLT does not cause any spot motion; only its tilt matters. This is different from the LGS projector of the Multiple Mirror Telescope where the LLT lens and the focal point source are located on different parts of the telescope structure and, as a result, the LGS position on the sky is more sensitive to vibrations.

The LLT is being designed with tight constraints on space and mass. This is why reflective optics were chosen. The primary mirror will be diamond turned from a light-weighted aluminum blank, with a total mass of only 1.3 kg but very small flexure, 8 nm r.m.s. after refocus. Another interesting feature of the LLT design is a small bore-sight camera permanently mounted behind the diagonal mirror. This mirror has a dielectric coating for 355 nm, so the light of a bright star can pass through it, to be detected by a CCD for pointing, focusing, and checks of the optical quality. The same optics will be used during LLT alignment.

4. PROJECT STATUS

The SAM project has passed preliminary design reviews of the main module (December 2005) and the LGS system (September 2007). The AO loop was closed in the laboratory for the first time in March 2005 using the real components (DM, WFS CCD, TurSim phase screens) in a prototype optical set-up and the real-time software.

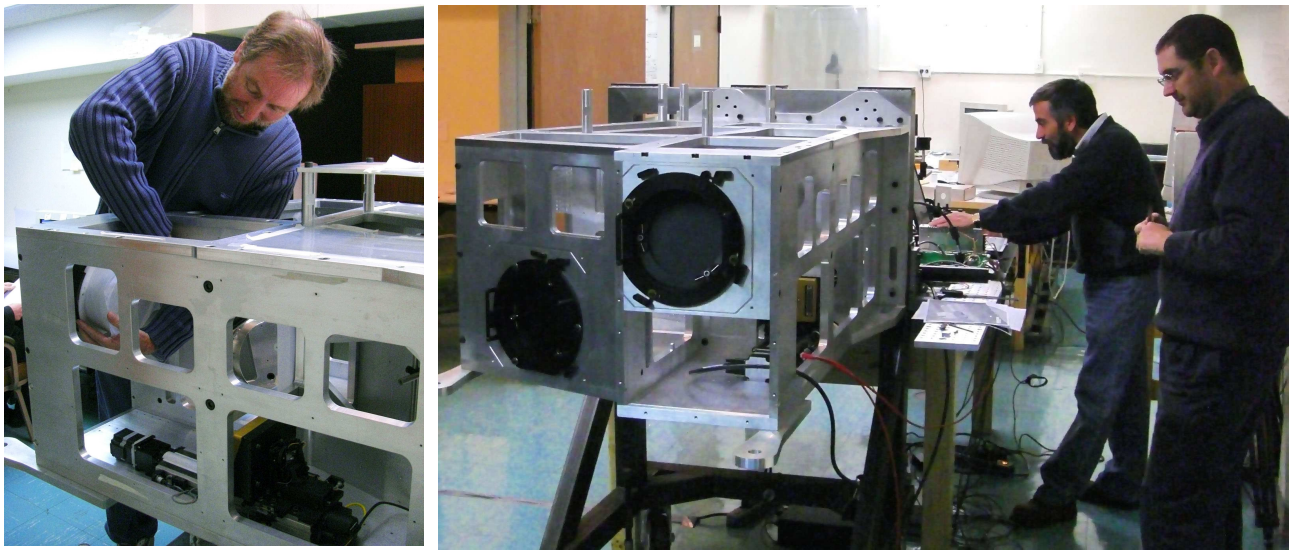

Figure 11. Integration and optical alignment of SAM (May 16, 2008).

Mechanical design has been the pacing item for the whole project. The integration of the main module started in March 2008, when the housing has been fabricated. The main optics is installed and aligned (Fig. 11). The NGS WFS module was assembled and functionally tested in closed loop using the prototype setup, then

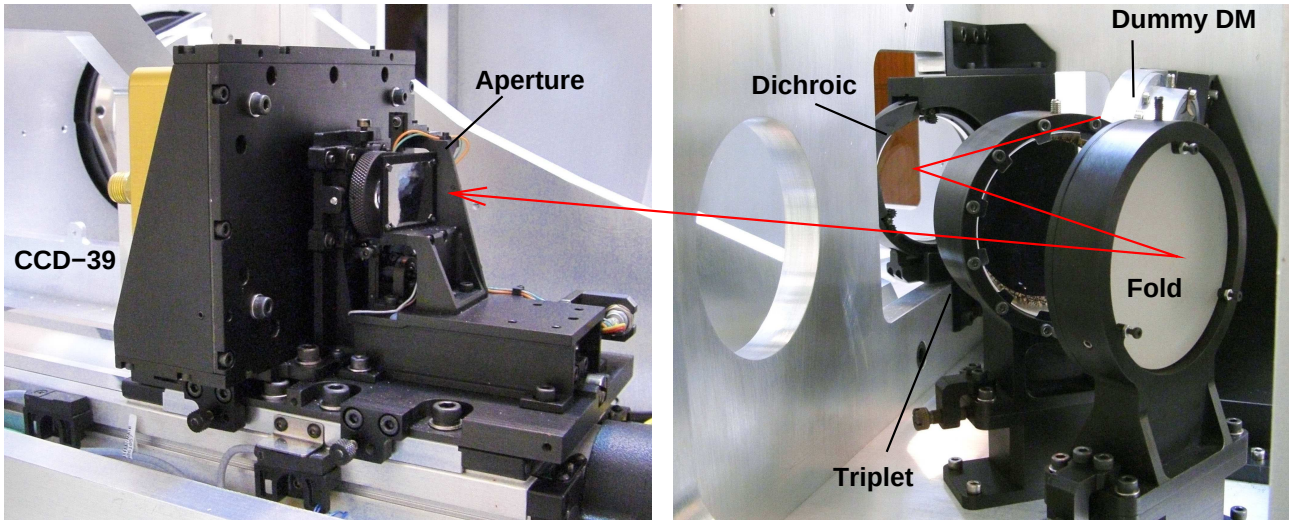

Figure 12. Ray path from the DM to the NGS WFS.

installed in the main module (Fig. 12). The TurSim, tip-tilt guider arms, and SAMI are not yet fabricated. All optics is received, while the laser and the CCD for SAMI are not yet ordered.

During 2008, the remaining sub-assemblies will be fabricated, tested, and installed. When the electronics and the motion control are functional, the AO module will be disassembled, to be re-integrated finally in the anodized housing. The commissioning of SAM in the NGS mode is planned for 2009. The design and fabrication of the LGS system will proceed in parallel. It is expected that the LGS mode will be operational within one year from the SAM first light, in 2010.

REFERENCES

[1] A. Tokovinin, B. Gregory, H. Schwarz, "Visible-light AO system for the 4.2-m SOAR telescope", *Proc. SPIE,* **4839,** pp. 673-680, 2003.

[2] A. Tokovinin, S. Thomas, B. Gregory, N. van der Bliek, P. Schurter, R. Cantarutti, E. Mondaca, "Design of ground-layer turbulence compensation with a Rayleigh beacon", *Proc. SPIE,* **5490**, pp. 870-878, 2004

[3] A. Tokovinin, "Performance and error budget of a GLAO system", these Proceedings.

[4] S. Thomas, T. Fusco, A. Tokovinin, M. Nicolle, V. Michau, G. Rousset, "Comparison of centroid computation algorithms in a Shack-Hartmann sensor", *MNRAS,* **371,** pp. 323-336, 2006